

4

Energetics of interlayer binding in graphite

The cohesive energy of a solid is commonly referred to as the energy required to “disassemble it into constituent atoms or molecules” [Israelachvili, 1992]. Determination of the cohesive energy, therefore, helps to understand the nature and magnitude of interactions that exist among constituent parts of a solid. In graphite, the prototype for layered materials, the description of total cohesive energy involves two fundamentally different types of interactions: the strong localized covalent bonds within a graphene sheet, and the weak non-local van der Waals (vdW) interaction between the layers [Pauling, 1948]. Consequently, graphite exhibits both high and weak bond strengths along different directions in same crystal. Due to this strong lattice anisotropy, the discrimination of the interlayer cohesive energy from the total cohesive energy is essential. Due to the extremely different magnitude and nature of interactions in graphite, the theoretical calculations of the interlayer cohesive energy using *ab initio* or semi-empirical methods have results ranging from as small as 8 meV/atom to as large as 200 meV/atom [Brennan, 1952; DiVincenzo et al., 1983; Lii and Allinger, 1989; Schabel and Martins, 1992; Trickey et al., 1992]. Even the use of the density functional theory, today’s standard tool for electronic structure calculations, has resulted in a range of values for interlayer cohesive energy [Charlier et al., 1994; Rydberg et al., 2003]. The poor description of interlayer cohesive energy in general is attributed to the types of electron correlations used within various theoretical techniques. For example, the electron correlation used within the density functional formalism is short-range [Kohn et al., 1998]. In contrast, the interlayer cohesive energy in graphite is largely dictated by long-range vdW interactions, and, therefore the use of density functional theory to define it is expected to lead to an inaccurate description [Kohn et al., 1998; Rydberg et al., 2003]. The

experimental determination of the interlayer cohesive energy, on the other hand, is comparatively rare and is restricted to the heat of wetting experiments by Girifalco and Lad [1956], and a measurement based on the radial deflation of multi-wall carbon nanotubes (MWNTs) [Benedict et al., 1998]. The interlayer cohesive energy obtained from above experiments are 43 and 35 meV/atom, respectively. As currently, the scarcity of experimental results as well as the considerable ambiguity in theoretically determined values imply that further experiments are necessary to provide additional evidence so that the comparison between theoretical and experimental values can be put on a solid footing.

A better understanding of long-range vdW forces in graphitic systems is also required for examining the interaction between carbon nanotubes. They are generally found to be agglomerated to form quasi-crystalline hexagonal bundles or ropes because of considerable long-range vdW interactions [Journet and Bernier, 1998; Thess et al., 1996]. These are quite similar to interactions in planar graphitic systems [Charlier et al., 1995]. Precise knowledge of the graphitic interlayer cohesive energy would be advantageous when studying the ordering and self-assembly of nanotube bundles and other similar vdW bonded sp^2 carbon networks.

In this chapter, an experimental characterization of the weak interlayer interactions in graphite is presented. The results arise from the thermal desorption of thin films of polyaromatic hydrocarbon molecules (PAHs) from the surface of highly oriented pyrolytic graphite (HOPG). Due to striking resemblance in structural as well as electronic characteristics of PAHs with graphene layer, i.e., the basal plane of graphite, the interaction of the former with graphite is considered to be the model system to represent graphene-graphene interactions. The binding energies of PAHs on graphite, as obtained from temperature programmed desorption, is utilized to calculate the contribution from individual carbon atoms, which, in the limit of infinitely large PAH molecules, would correspond to the energy required to separate a graphene sheet from its parent crystal. The binding energy of non-polar molecules, like PAH molecules, can be attributed to long-range vdW interactions as indicated by the linear dependence on the static polarizabilities of PAH molecules. This chapter begins with a brief introduction to the structure and energetics of interlayer binding in graphite. Subsequently, the binding energies of PAH molecules on graphite are dealt with. The interlayer cohesive energy is deduced by optimizing the experimentally obtained PAH binding energies with carbon-carbon and carbon-hydrogen interaction potentials using MM3 force fields.

4.1. Graphite: Structure and properties

Graphite, considered as ‘the prototype’ for the van der Waals bonded solids, exhibits a well-developed layer structure, with a strong lattice anisotropy. In this section, the lattice and electronic structures of graphite are presented. As discussed below,

the electronic properties of graphite are strongly influenced by the anisotropy in the lattice structure.

4.1.1. Lattice structure

The crystal lattice of graphite consists of an ordered stacking of basal planes where carbon atoms within the planes form open hexagons. Each carbon atom is trigonally bonded to three nearest neighbors within the plane through sp^2 ($2s-2p_x-2p_y$) hybridized orbitals. The resulting strong covalent (σ) bonds have a short interatomic distance, 1.41 Å. The overlap of unhybridized $2p_z$ orbitals from each carbon atom additionally leads to the formation of π bonds. The stacking order of basal planes, as observed in the natural graphite, presents two cases of close packed structures: hexagonal structure and rhombohedral structure.

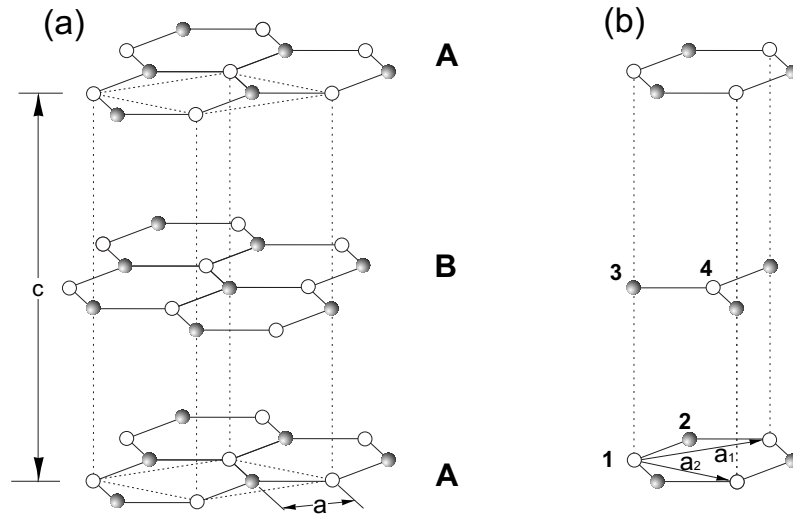


Figure 4.1.: Left panel shows the crystal structure of hexagonal graphite. Each carbon atom within the basal plane is covalently bonded to three nearest neighbors (illustrated with gray and white spheres) through 3 sp^2 hybridized σ orbitals and an unhybridized $2p_z$ orbital. The resulting interatomic distance is 1.41 Å. The stacking of the layers as ABAB pattern in hexagonal graphite is due to weak interplanar interactions between π electrons in the adjacent planes. The unit cell of the graphite is indicated by the broken line. (b) Unit cell has four different carbon atoms marked 1, 2, 3 and 4 shown in the right panel.

In hexagonal graphite, the basal planes are stacked in an **AB** fashion [Fig. 4.1(a)]. Here, the atoms in the planes denoted by same letter are in exact register, and those in other planes fall into the two possible sets of neighboring sites. The unit cell of the hexagonal close-packed structure has four carbon atoms [marked 1, 2, 3 and 4 in Fig. 4.1(b)]. The ordering of layers in rhombohedral graphite has an

ABC sequence. The stacking of basal planes in graphite is **AB** or **ABC**, due to weak interactions between layers derived from the unhybridized $2p_z$ orbitals. This weaker interaction has a spacing of 3.35 Å between the basal planes [Reynolds, 1968]. The interaction between the basal planes of graphite is largely dominated by long-range van der Waals interaction which originates from the correlated motions of electrons in different planes. Because of these two fundamentally different kinds of interactions, i.e., covalent and van der Waals along different crystal directions, the lattice structure of graphite is extremely anisotropic and is unusual in showing both highest and lowest bond strengths in different directions in the same crystal [Delhaes, 1998].

4.1.2. Interlayer cohesive energy of graphite

The theoretical calculation of graphitic electronic structure was pioneered by Wallace [1947]. In order to characterize the binding within the basal planes, he used a “tight-binding approximation”. With this approximation, the electronic structure is calculated by separating the interaction within each basal planes (covalent) from in-plane interactions (van der Waals). Such a separation is justified due to the weak interaction that exists between graphene sheets. The linear combinations

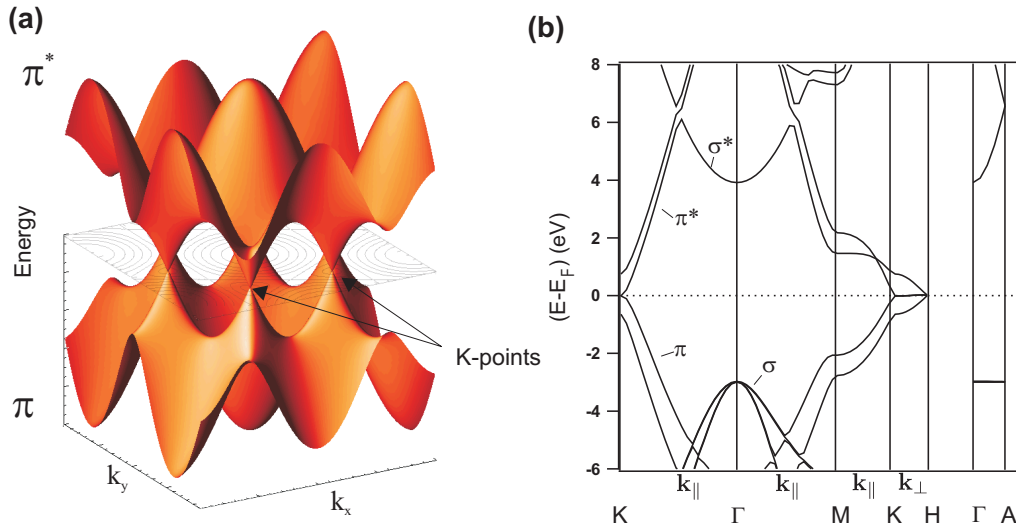


Figure 4.2.: (a) The π bonding and π^* anti-bonding orbitals of an isolated graphene sheet show a zero-gap semiconductor as predicted by the tight-binding approximation. (b) Corresponding electronic band structure of graphite along major symmetry points. The non-zero slope of these bands (π and π^*) along the $K-H$ (\mathbf{k}_\perp) direction indicate a strong dispersion along the c -direction in the graphitic crystal.

of hybridized sp^2 orbitals and unhybridized $2p_z$ orbitals are used to obtain the

σ and π bands in an isolated graphene sheet. The calculations involving tight-binding approximation have shown that an isolated graphene sheet is a zero-gap semiconductor, which is explained by the degeneracy of π and π^* at the K -point Fig. 4.2(a).

3D- Brillouin zone

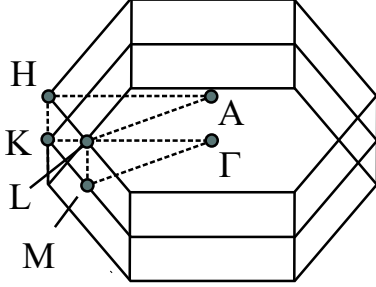


Figure 4.3.: First Brillouin zone of three-dimensional graphite with all high symmetry points.

In Fig. 4.3 the three-dimensional Brillouin zone of graphite showing all high symmetry points is displayed. The corresponding electronic band structure along the various high symmetry points is shown in Fig. 4.2(b). Normal to the basal planes (i.e., the along K - H direction in Fig. 4.2) there is only a slight or no dispersion of the σ bands. However, the π bands show some dispersive character [Wallace, 1947]. This dispersion in the π bands is clearly indicated in the electronic band structure as the non-zero slope of π and π^* bands along the \mathbf{k}_\perp direction [Fig. 4.2(b)].

The origin of the dispersion is believed to be due to the correlated interactions between the electrons in different planes, and is strong enough to cause the stacking of graphene sheets as in graphite crystal [Charlier et al., 1994; Reynolds, 1968]. In terms of electronic structure, the long-range interaction between the electrons in different layers is strong enough to remove the aforementioned degeneracy in the π and π^* bands, which makes graphite a semi-metal [Wallace, 1947]. However, this interaction, and hence corresponding binding energy, is considerably weaker in comparison to localized, in-plane, covalent interactions. As mentioned in the beginning of this chapter, attempts to calculate interlayer binding energy using methods such as semi-empirical or even density functional theory (DFT) have yielded a large range of values from 8 meV/atom to about 200 meV/atom (see Table 4.1). This diversity in the calculated value of interlayer cohesive energy is due to the poor representation of the long-range interactions that dominate the interlayer cohesive energy [Rydberg et al., 2003; Schabel and Martins, 1992; Wang et al., 2000]. For instance, within the density functional formalism the cohesive energy of solids is described in terms of the total energy (E_{tot}). The latter being a function of electron density ($[n(\mathbf{r})]$), is given by:

$$E_{tot}[n(\mathbf{r})] = T[n(\mathbf{r})] + U[n(\mathbf{r})] + E_{xc}[n(\mathbf{r})].$$

Here $T[n(\mathbf{r})]$ is the kinetic energy, $U[n(\mathbf{r})]$ is the potential energy and $E_{xc}[\mathbf{r}]$ is the exchange-correlation energy [Charlier et al., 1994; Kohn and Sham, 1965]. The van der Waals interaction is ‘hidden’ in the correlation part of the exchange-correlation energy. Unfortunately, the exact exchange-correlation energy is not known, and one usually uses a short-range exchange correlation in the local-density approximation

(LDA) [Charlier et al., 1994; Jones and Gunnarsson, 1989]. However, the short-ranged correlations are inappropriate to describe vdW interactions between adjacent graphene sheets, as the dynamic correlations between electrons in these sheets are long-range. Thus, if DFT is to be used to obtain interlayer cohesive energy, it is apparent that the calculated value will be dominated by the short-range covalent interactions that exists within the basal plane [Kohn et al., 1998].

Table 4.1.: Summary of interlayer cohesive energy E_{ex} of graphite obtained by various theoretical and experimental methods (in the unit of meV/atom).

E_{ex}	Method	Reference
<i>Theoretical</i>		
8	DFT-LDA	Charlier et al. [1994]
30	DFT-LDA	Trickey et al. [1992]
113	Molecular Mechanics	Lii and Allinger [1989]
24	DFT-nonlocal	Rydberg et al. [2003]
191	DFT-LDA	DiVincenzo et al. [1983]
25	DFT	Schabel and Martins [1992]
200	Semiempirical	Girifalco and Lad [1956]
<i>Experimental</i>		
43	Heat of wetting	Girifalco and Lad [1956]
35	Deflation of MWNTs	Benedict et al. [1998]

In contrast, the experimental characterization of the graphitic interlayer binding energy, has been relatively scarce. It is restricted to heat of wetting experiments by Girifalco and Lad [1956] and a measurement based on the deflation of ‘bulbs’ at the end of MWNTs [Benedict et al., 1998]. The measurement of heat of wetting resulted in a value of 43 meV/atom. However, an assessment of sample dependent and other uncertainties of this characterization is not possible, as the nature of carbon materials used in that experiment is relatively unknown. Carbon powders commonly used for such experiments usually have high surface areas, i.e., of the order of few 10s to 100s of square meters per gram. They are generally treated with acids to oxidize any non-graphitic contaminants and then thermally treated to achieve the highest possible degree of graphitization [Reynolds, 1968]. The adsorptive as well as wetting properties of such samples depend critically on the thermal history of the sample treatment [Ehrburger and Vix-Guterl, 1998]. Also problematic is that the corresponding data is published in a thesis and not readily available [Girifalco and Lad, 1956]. The second measurement is based on the collapse of bulbs at the ends of MWNTs and resulted in (35^{+15}_{-10}) meV/atom for the interlayer binding energy

[Benedict et al., 1998]. The radius of nanotubes used is determined with an accuracy of 1–2 Å. Again, also, the measurement is limited by the inaccuracies in determining the bulb diameter.

4.1.3. Polyaromatic hydrocarbons on graphite: The model system

Polyaromatic hydrocarbons are a class of planar aromatic molecules formed by the fusion of two or more aromatic rings. They are formally regarded as ‘two-dimensional graphite sections’ due to their striking similarity with the basal plane of graphite. Therefore, they serve as a suitable model system to investigate the interlayer cohesive energy in graphite. ‘All-benzenoid PAHs’ are polyaromatic molecules with all hexagonal or benzene-like rings and have played an important role in developing the theory of graphite [Müller et al., 1998]. The structural similarity between PAHs and a graphene sheet is evident by the similar hybridization of all carbon atoms (sp^2). Additionally, the bond distances in higher PAHs, such as coronene or ovalene, is found to be between 1.40 and 1.42 Å; a value very close to the interatomic distance in graphite, 1.41 Å. [Clar, 1964; Robertson and Trotter, 1961].

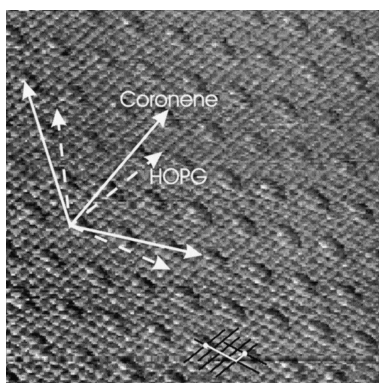


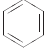
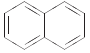
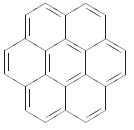
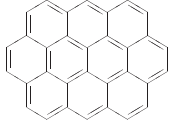
Figure 4.4.: Simultaneous visibility of coronene (adsorbate) and graphite (substrate) in the scanning tunnelling microscopy (STM) picture demonstrates the commensurate monolayer structure of PAHs on graphite surface. Picture is adapted from [Walzer et al., 1998].

Further, experiments such as low energy electron diffraction and scanning tunnelling microscopy have demonstrated that at lower coverages (roughly of 1 ML, ML = monolayer), PAH molecules form a commensurate monolayer with a configuration in which their molecular plane remains parallel to the graphite surface [Bardi et al., 1987; Gameson and Rayment, 1986; Walzer et al., 1998; Zimmermann and Karl, 1992]. In Fig.4.4., an example of a commensurate monolayer of coronene adsorbed on HOPG is depicted. The tendency of the PAH molecules to form lamellar structures is also illustrated in theoretical studies [Vorpagel and Lavin, 1992]. This planar configuration is analogous to the stacking of basal planes in graphite. Also, the interlayer distance between the molecular planes in large PAH molecules in the crystal is very close to the interlayer separation of graphite [Robertson and White,

1945]. Finally, the electronic structure calculation of PAH clusters indicates that the density of states in larger PAHs converges to that of graphite, and therefore, the electronic structure of the PAHs provides a good approximation of energy states of bulk graphite [Ruuska and Pakkanen, 2001].

Our aim here is to utilize the above similarities between the PAHs and the basal plane of graphite to experimentally characterize the interlayer binding energy in graphite. For that purpose, the interactions of four polyaromatic hydrocarbons: benzene, naphthalene, coronene and ovalene (Table 4.2), with the basal plane of graphite are studied using thermal desorption spectroscopy (TDS). The activation energy of PAHs on graphite obtained from the TDS measurement is then used to derive the contribution due to each carbon atom, which, in the limit of an infinitely large PAH, would correspond to interlayer cohesive energy of graphite.

Table 4.2.: Molecular structure and properties of four polyaromatic hydrocarbons used in the experiment

Name	Formula	Mol.wt.(g mol ⁻¹)	$\langle\alpha\rangle(\text{\AA}^3)$	$\alpha_{zz}(\text{\AA}^3)$	Structure
Benzene	C ₆ H ₆	78.11	10.18	4.17	
Naphthalene	C ₁₀ H ₈	128.17	17.65	6.44	
Coronene	C ₂₄ H ₁₂	300.35	44.85	13.50	
Ovalene	C ₃₂ H ₁₄	398.46	59.75	19.70	

4.2. Desorption kinetics of polyaromatic hydrocarbons

In this section, the experimental aspects of the TD of polyaromatic hydrocarbons from the basal plane of graphite is described. Analysis of thermal desorption (TD) traces are performed using the Falconer-Madix method and Redhead's peak maximum method [Falconer and Madix, 1977; Redhead, 1962]. The activation energies of desorption, and pre-exponential frequency factors are obtained using the first method. The second method is based on the evaluation of the temperature corresponding to the maximum desorption rate. Calculation of the activation energy applying this method uses an assumed value of the pre-exponential. In our experiments, these pre-exponentials are obtained from the temperature dependence of PAH vapor pressures, by the extrapolation of the available vapor pressure data to the respective desorption temperatures using Antoine's fit. The experimentally determined binding energies of PAHs on graphite are then shown to be dependent on the respective molecular static polarizabilities in a linear fashion.

4.2.1. Temperature programmed desorption of PAHs

The HOPG sample (Grade ZYB, Advanced Ceramics) used for the thermal desorption experiments was freshly cleaved and mounted on a tantalum disk using conducting silver epoxy (see chapter 3 for additional details of the procedure). Thereafter, before each dosing, the sample surface is cleaned by annealing up to 1100 K, and then the sample surface is cooled down to 30 K by means of a continuous liquid helium cryostat attached to the sample holder. The temperature of the sample surface is monitored using a *K*-type (Chromel-Alumel) thermocouple attached to the tantalum disk. The calibration of thermocouple is carried out using Xe multilayer desorption from HOPG [Ulbricht et al., 2003]. All desorption experiments are carried out under ultrahigh-vacuum (UHV) conditions where a base pressure better than 2×10^{-10} mbar is maintained.

For dosing, a predetermined quantity of benzene or naphthalene (99.89 % and 99.99 %, Aldrich) vapor is released from a gas reservoir to the sample surface through a retractable pin hole doser. Prior to the exposure of adsorbents, unwanted atmospheric contaminants (dissolved gases such as oxygen, nitrogen etc.) are removed by freeze-pump cycles. The exposure of coronene (99 %, Aldrich) and ovalene (99.5 %, Dr. Ehrenstorfer GmbH) is carried out by the sublimation of the powder material from a proportional-integral-differential (PID) temperature controlled Knudsen cell. A typical coverage series is obtained by dosing the graphite surface with successively increasing adsorbate quantities up to a total coverage of approximately 10 L. The desorption data corresponding to the species with mass-to-charge ratio of up

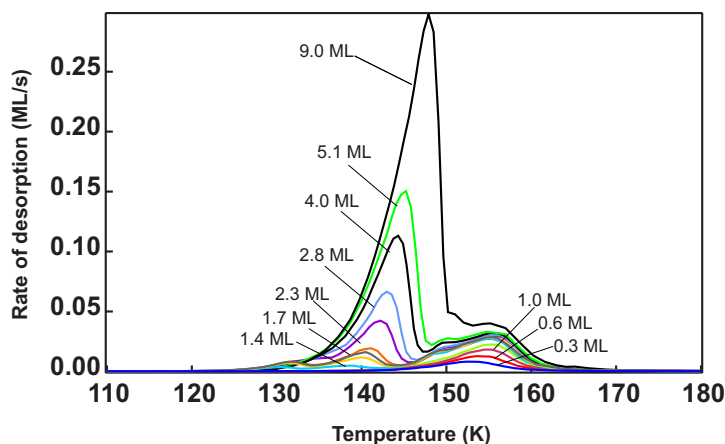


Figure 4.5.: Series of thermal desorption spectra of benzene from HOPG surface. The heating rate used for desorption is 0.75 K s^{-1} . Initial surface coverages are expressed here in units of close-packed monolayer of benzene on HOPG, and are indicated by the arrows.

to 200 a.m.u/e, such as benzene and naphthalene, are acquired using a quadropole mass spectrometer. The desorption of higher molecular masses, such as coronene

and ovalene, are acquired by monitoring the total pressure inside the UHV chamber using a Bayard-Alpert ionization gauge. When the mass spectra corresponding to coronene and ovalene are acquired, the TD traces are background corrected by carefully cross-checking with the simultaneously recorded TD spectra from species with masses between 4 and 200 a.m.u.

Figure 4.5 displays a series of TD spectra of benzene desorption from HOPG after exposing the surface with a coverage of up to 10 close-packed monolayers (10 ML). The TD spectra are recorded using a heating rate of 0.75 K s^{-1} . The spectra are characterized by a high temperature feature centered at 152 K, which is attributed to the desorption from the first monolayer. Additionally, a low temperature feature centered at 141 K is observed with increasing coverage and is ascribed to the desorption from multilayers. At coverages near 1 ML, an additional peak appears at 132 K (see the sub-monolayer region in Fig. 4.6).

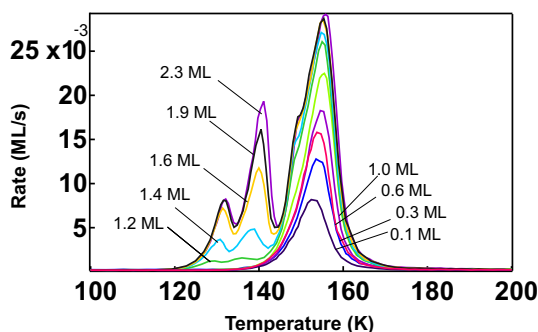


Figure 4.6.: Desorption features of benzene from graphite surface in the sub-monolayer region. In addition to the peaks arising from the mono- and multilayer desorptions, when the surface coverage approaches saturation monolayer coverage, a peak attributed to the different configurational phases is seen at 132 K.

the complex sub-monolayer phase diagram of benzene, which exhibits coverage and temperature dependent orientational features.

At coverages significantly below 1 ML and at 152 K, i.e., the temperature corresponding to the desorption in our experiments, benzene is found to form a two-dimensional, commensurate monolayer [Bardi et al., 1987; Meehan et al., 1980]. In this configuration, the benzene molecules are oriented with their molecular plane parallel to the basal plane of graphite. This ‘face-to-face’ orientation is schematically shown in Fig. 4.7(a). With increasing temperature, molecules gain orientational freedom and tend to orient themselves with their molecular plane perpendicular (or tilted) to the basal plane [Fig. 4.7(b)]. This perpendicular phase has a lower binding energy on the surface when compared to the face-to-face type

The temperature corresponding to the maximum desorption rate, i.e., T_{max} for the monolayer desorption rate shifts only by 2–3 K (for clarity, see Fig. 4.6) and is therefore independent of the initial coverage. The coverage independent peak maximum as well as the shape of monolayer desorption peaks confirm first-order kinetics, which is typical for molecular adsorption on graphite surfaces [Ulbricht et al., 2002a]. With increasing surface coverage, the additional peak that appears at 135 K merges with multilayer desorption peaks. The evolution of this peak can be explained using the

of orientation [Vorpapel and Lavin, 1992]. The transition from the face-to-face orientation to the perpendicular orientation is also influenced by the surface coverage. For simpler PAH molecules, such as benzene, as the coverage approaches 1 ML, the tilted phase is preferred so as to satisfy steric and entropic constraints [Tabony et al., 1980]. This is particularly true for smaller molecules, for which the energy difference between face-to-face and perpendicular orientation is small enough to cause the transition at desorption temperatures [Vorpapel and Lavin, 1992]. On the other hand, for bigger PAHs such as coronene, even at higher coverages the preferred phase is with face-to-face orientation [Vorpapel and Lavin, 1992]. Thus, with the coverage approaching the monolayer regime, the desorption traces broaden towards the low temperature range – as is expected due to changes in the molecular orientation within the adsorbate layer at higher coverages. The TD spectrum from a complete monolayer is here associated with the last trace, before the multilayer desorption feature develops at around 141 K with increasing coverage. This is typical of desorption from multilayers with a common leading edge which corresponds to zero-order kinetics. Analogous to the desorption kinetics

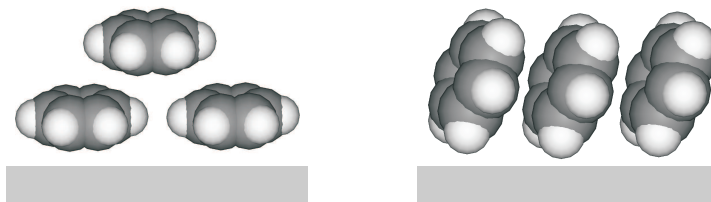


Figure 4.7.: Schematic illustration of coverage dependent configurations of benzene molecules on graphite surface. (a) At coverage less than a saturated monolayer coverage, benzene molecules have a face-to-face orientation in which molecules remain with their molecular plane parallel to the HOPG. (b) With coverages approaching a saturated coverage, molecules will prefer an orientation with their molecular planes perpendicular (or tilted) to the surface so as to satisfy the steric and entropic constraints.

of benzene, the naphthalene desorption spectra (Fig.4.8) exhibit two clearly distinguishable features corresponding to mono- and multilayer desorptions, centered at 235 and 210 K, respectively. These spectra are recorded using a heating rate of 1 K s^{-1} . The TD traces also exhibit a temperature independent peak maximum, which indicates that the desorption of the naphthalene monolayer follows a simple first-order kinetics, similar to the monolayer desorption of benzene. However, unlike the desorption spectra of benzene, the naphthalene TD spectra are not complicated by additional peaks due to phase transitions, such as a parallel to perpendicular transition. The orientation of naphthalene molecules on the graphite surface have been studied using low energy electron diffraction (LEED) which indicates that naphthalene exhibits two distinct, coverage dependent, monolayer phases [Bardi

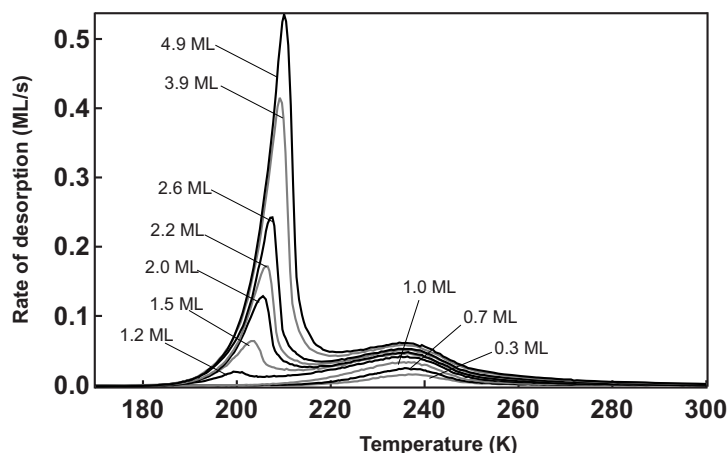


Figure 4.8.: Series of thermal desorption spectra of naphthalene from HOPG surface after exposing the surface to a coverage of up to 5 close-packed monolayers. The initial surface coverages of the traces are indicated by arrows. The heating rate used for the desorption is 1 K s^{-1} .

et al., 1987]. However, the low and high-coverage phases differ in dimension and geometry of their unit cell, and have their molecular planes parallel to the graphitic surface. Therefore, these phases have similar binding energies and cannot possibly be resolved using the thermal desorption spectroscopy.

Figures 4.9 and 4.10 display the TD spectra of coronene and ovalene after the surface was exposed to a coverage of roughly 8 ML. The spectra are collected for a heating rate of 2 K s^{-1} . The similarity of these adsorbents with the substrate (HOPG) is evident by the absence of clearly distinguishable mono- and multilayer desorption features. For coronene desorption, the monolayer desorption peak appears initially at 390 K and shifts to higher temperatures with an increased surface coverage. For ovalene, the same monolayer peak appears at 490 K, and similar to the coronene, as the initial surface coverage is increased, the peak is seen to shift to higher temperatures. These desorption features of coronene and ovalene are typical of the fractional-order desorption kinetics. The fractional-order desorption observed for coronene or ovalene can be attributed to the formation of two-dimensional islands which are stable up to desorption temperatures in our experiments. For example, Walzer et al. [1998] have observed that bigger PAH molecules agglomerate on graphite surface to form ‘puddles’ or two-dimensional islands, often having a circular shape. Such islands are stable up to typical desorption temperatures due to the considerable lateral interactions among the adsorbents. Because of a lower coordination of adsorbates along the edges of these islands, the removal of adsorbents during desorption takes place preferably from the circumference of islands and, as a result, will have fractional-order desorption kinetics [Arthur and Cho, 1973]. For coronene and ovalene desorption, the saturation

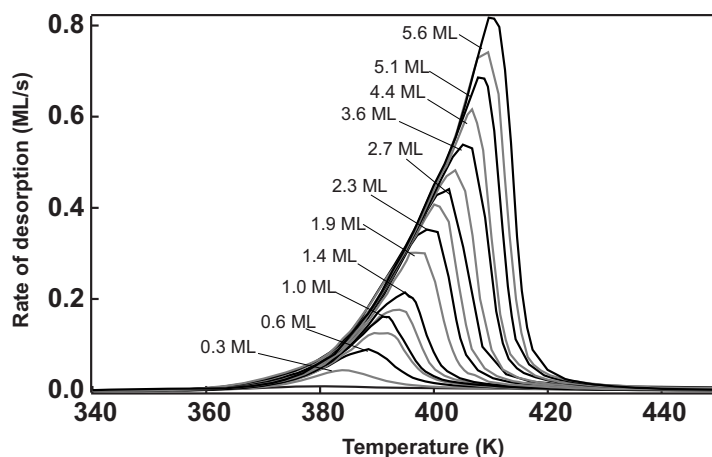


Figure 4.9.: Series of thermal desorption spectra of coronene from HOPG surface after exposing the surface to a coverage of up to 5 close-packed monolayers. The initial surface coverages of the traces are indicated by arrows. The heating rate used for the desorption is 2 K s^{-1} .

coverage is estimated from the development of a common leading edge in the TD spectra. Also, for the ovalene desorption, additional verification of the saturation coverage is indicated by a small shoulder-like feature that appears around 505 K.

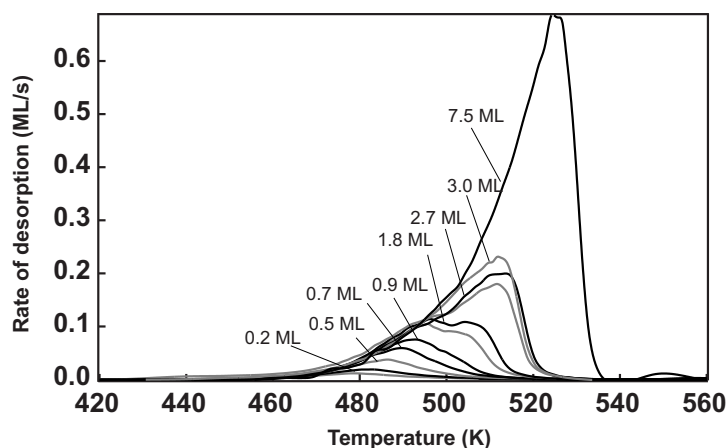


Figure 4.10.: Series of thermal desorption spectra of ovalene from HOPG surface after exposing the surface to a coverage of up to 8 close-packed monolayers. The initial surface coverages of the traces are indicated by arrows. The heating rate used for the desorption is 2 K s^{-1} .

4.2.2. Determination of frequency factors and binding energies

The rate of desorption of any adsorbate from a solid surface, as measured above, can be described using the Arrhenius equation:

$$-\frac{d\theta}{dt} = \nu\theta^n \exp\left(-\frac{E_d}{k_B T}\right), \quad (4.1)$$

where $(d\theta/dt)$ is the rate of desorption, ν is the pre-exponential frequency factor, θ is the surface coverage and E_d is the activation energy for desorption. Eq. (4.1) is evaluated in the following calculations to obtain the activation energy of desorption using a peak maximum method (Redhead method) and the Falconer-Madix method (for details of these methods, see chapter 3) [Falconer and Madix, 1977; Redhead, 1962].

In the Redhead method, the activation energy E_d is linearly related to the temperature of the desorption peak maximum T_{max} , and the heating rate β :

$$E_d = k_B T [\ln(\nu T_{max}/\beta) - 3.64]. \quad (4.2)$$

The application of the above equation is most commonly used for analysis of TD spectra for systems that follow first-order kinetics (i.e., monolayer desorption of benzene and naphthalene). However, the method can be extended to the evaluation of desorption parameters for fractional- or zero-order kinetics if the desorption trace used for the determination of the T_{max} corresponds to the evaporation from a saturated monolayer. As indicated by Eq. (4.2), the crucial factor for the analysis of TD spectra using Redhead's peak maximum method is the availability of a reliable pre-exponential frequency factor ν . Usually, they are assumed to be on the order of 10^{12} to 10^{15} s^{-1} , and small uncertainties of an order of magnitude or less will not give rise to any serious error in the resulting activation energies [Christmann, 1991]. However, the assumption of constant pre-exponentials may introduce considerable error into the activation energy calculation, in particular if the desorption of large adsorbates with many internal degrees of freedom are studied [Fichthorn and Miron, 2002; Paserba and Gellman, 2001a,b]. This has been shown for the thermal desorption of long alkane chains from graphite [Paserba and Gellman, 2001a]. The pre-exponential factors for their thermal desorption were calculated using the transition state theory (TST) and were found to increase by four orders of magnitude with increasing chain length (from 10^{12} s^{-1} for methane up to 10^{16} s^{-1} for $\text{C}_{12}\text{H}_{26}$ [Fichthorn and Miron, 2002]). Quantitatively, this is attributed to the constraints on the various vibrational degrees of freedom of the molecule in the adsorbed state. If the pre-exponentials are calculated using TST, one usually also computes the ratio of partition functions in the adsorbed and the transition states. Therefore, if the molecular degrees of freedom are constrained or 'frozen' in the adsorbed state, as is the case for larger PAH molecules, the growing differences between the adsorbed

and the transition state will often reduce the corresponding partition functions and thus tend to yield higher pre-exponential factors [Christmann, 1991]. Thus, in the analysis of polyaromatic hydrocarbon TD spectra, assuming the value of the pre-exponentials is avoided in order to minimize errors.

For the following calculations, the pre-exponential frequency factors are instead calculated from the temperature dependence of PAH vapor pressures. This is done by assuming a detailed balance of adsorption and desorption rates between the multilayer film in equilibrium with its gas-phase vapor. Here, one assumes that the pre-exponential factors do not depend strongly on the film thickness, and therefore, the values obtained for multilayers can be used in the analysis of monolayer desorption rates [Schlichting, 1990]. The detailed balance between the adsorption and desorption rates is done by equating the adsorption process as a condensation process. From the kinetic theory, the rate of adsorption $rate_{ads}$ can be expressed as [Eyring et al., 1962]:

$$rate_{ads} = \frac{s p(T)}{\sqrt{2\pi m k_B T}}, \quad (4.3)$$

where, $p(T)$ is the pressure of the gas at temperature T , s is the sticking probability and m is the mass of a single adsorbent molecule. Likewise, the rate of desorption of multilayers ($rate_{des}$) is expressed as the rate of vaporization:

$$rate_{des} = \nu \sigma \exp(-\Delta H_s/k_B T). \quad (4.4)$$

Here, σ is the number of adsorbates per unit area, ν is the frequency factor, and ΔH_s is the sublimation enthalpy of the adsorbate. Equating the right-hand sides of Eqs. (4.3) and (4.4), and using the Clausius-Clapeyron equality [Eq. (4.6)], the frequency factor is given by:

$$\nu = \frac{s}{\sigma \sqrt{2\pi m k_B T}} p_0, \quad (4.5)$$

where, p_0 is the vapor pressure as the $T \rightarrow \infty$ in Eq. (4.6). The σ of benzene, naphthalene and coronene molecules adsorbed on a graphite surface are obtained from the LEED or scanning tunnelling microscopy (STM) data [Bardi et al., 1987; Walzer et al., 1998] and are displayed in Table 4.3. For ovalene, where no such data are available, the σ is evaluated assuming that the molecules are close-packed with the polyaromatic rings oriented parallel to the surface. The vapor pressure p_0 is obtained from the temperature dependence of the vapor pressure calculated from the integrated Clausius-Clapeyron equation:

$$p(T) = p_0 \exp\left(-\frac{\Delta H_s}{k_B T}\right). \quad (4.6)$$

Here, ΔH_s is the heat of sublimation at the temperature of desorption T_{max} and p_0 is the pressure as $T \rightarrow \infty$. However, none of the vapor pressure curves of polyaromatics reported in the literature is extended to the range of desorption temperatures in

our TD experiments [de Kruif, 1980; Oja and Suuberg, 1998]. Due to the commonly observed increase in ΔH_s with decreasing temperature, the corresponding vapor pressures are obtained by extrapolation of vapor pressure data using Antoine's expression [Antoine, 1888]:

$$\ln [p(T)] = A - \frac{B}{T + C}, \quad (4.7)$$

where A, B, and C are the fit coefficients and are displayed in Table 4.3. Figure 4.11

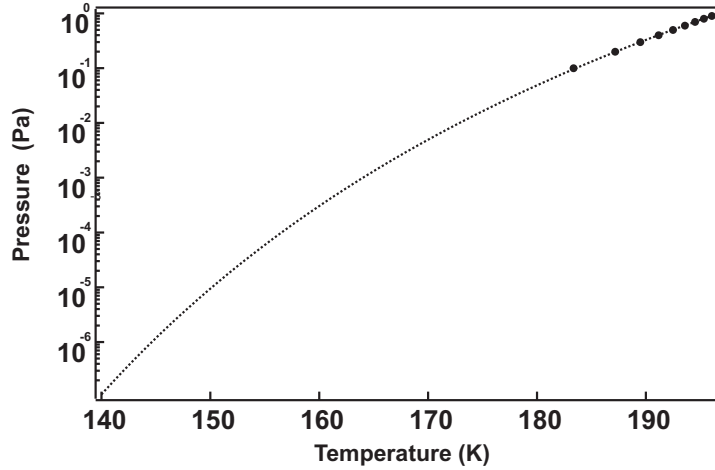


Figure 4.11.: Vapor pressure data of benzene and the extrapolation of the data to the benzene desorption temperature (152 K) using Antoine's fit function [Eq. (4.7)]. The fit coefficients A, B and C are listed in Table 4.3. The data is reproduced from de Kruif [1980].

displays a plot of the benzene vapor pressure data and the extrapolation of the data to the desorption temperature (see the Appendix A for a compilation of vapor pressure curves and their extrapolations for other polyaromatic hydrocarbons). The sticking coefficient, s , in Eq. (4.5) is assumed to be close to unity, as is commonly observed for homo-epitaxial growth, and should be appropriate for the adsorption of weakly interacting polyaromatics on graphite. The pre-exponential frequency factors and activation energy of desorption are computed using Eq. (4.5) and are presented in Table 4.4. For ovalene, where no vapor pressure data are available, the pre-exponential factor $5.6 \times 10^{21} \text{ s}^{-1}$ is obtained using the tabulated slope and offset from Clausius-Clapeyron equation in the form $\ln(p) = A - B/T$ [Inokuchi et al., 1952]. The calculated value of pre-exponential factors are displayed in Table 4.4. The pre-exponentials are then used in Eq. (4.2) and the corresponding activation energies are obtained (Table 4.4).

The calculation of activation energies and pre-exponential frequency factors using the method proposed by Falconer and Madix [1977] is based on the evaluation of thermal desorption curves under a set of constant temperatures. This method provides constant temperature-kinetic information, as seen in an isothermal desorption

Table 4.3.: Compilation of Antoine's fit coefficients and desorption temperature of the four polyaromatic hydrocarbons.

Molecule	A	$B(K)$	$C(K)$	$\sigma(\text{cm}^{-2})$	$p_0(\text{mbar})$	$T_{max}(K)$
Benzene	26	7640	30	2.7×10^{18}	5.8×10^{11}	152
Naphthalene	43	20100	124	1.6×10^{18}	1.3×10^{14}	235
Coronene	37	30400	184	0.9×10^{18}	2.6×10^{13}	390
Ovalene	-	-	-	0.6×10^{18}	7.6×10^{13}	490

experiment. In employing this procedure, it is not necessary to calibrate the surface coverage in terms of a saturation monolayer as long as consistent units are used for a set of experimental curves. To analyze the TD spectra using the Falconer-Madix method, the *logarithm of desorption rate* $[\ln(-d\theta/dt)]$ is plotted versus the *logarithm of the surface coverage* $(\ln \theta)$ for constant temperatures and for desorption traces from different initial coverages. This is repeated for several temperatures. The desorption parameters are then obtained from these *log-log* plots according to the following equation:

$$\ln \left(-\frac{d\theta}{dt} \right) = \ln(\nu) + n \ln(\theta) - \frac{E_d}{k_B T}. \quad (4.8)$$

As shown in Eq. (4.8), the isothermal desorption plots are a set of straight lines if the activation energy is independent of the surface coverage. Here I assume that the activation energies do not change considerably over the coverage range used for the analysis using Falconer-Madix method. Therefore, the isotherms are constructed

Table 4.4.: Comparison between the activation energies of desorption and the pre-exponential frequency factors of polyaromatic hydrocarbons desorbed from a graphite surface obtained by using the Redhead's peak maximum method and the Falconer-Madix method.

	Redhead		Falconer-Madix	
	$\nu(\text{s}^{-1})$	$E_d(\text{eV})$	$\nu(\text{s}^{-1})$	$E_d(\text{eV})$
Benzene	$9.0 \times 10^{15 \pm 3}$	0.50 ± 0.08	$5.4 \times 10^{15 \pm 2.2}$	0.50 ± 0.08
Naphthalene	$5.5 \times 10^{16 \pm 2}$	0.80 ± 0.09	$9.8 \times 10^{16 \pm 1.6}$	0.90 ± 0.07
Coronene	$2.4 \times 10^{16 \pm 2}$	1.32 ± 0.16	$1.7 \times 10^{18 \pm 0.5}$	1.48 ± 0.06
Ovalene	$5.1 \times 10^{21 \pm 3}$	2.20 ± 0.19	$8.1 \times 10^{18 \pm 0.5}$	1.97 ± 0.04

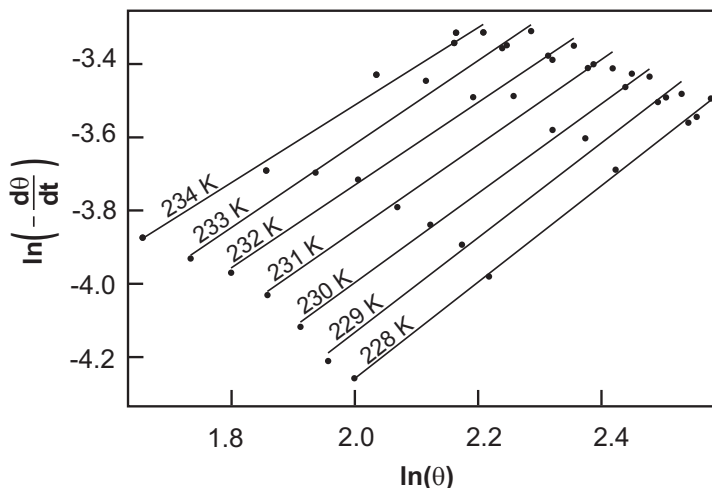


Figure 4.12.: Isothermal desorption plots (*logarithm of rate versus logarithm of surface coverage*) and linear fits to isotherms for benzene desorption from HOPG surface. Isotherms are constructed for the temperature range of desorption, i.e., from 225 to 235 K using traces corresponding to the sub-monolayer desorption.

for the temperatures in the range of monolayer desorption. Typical isothermal desorption plots for benzene obtained in a temperature range of 225 and 235 K are displayed in Fig. 4.12. The order of PAH desorption, n , is derived from the slope of a linear fit to the isotherm according to Eq. (4.8). The slope of the linear fit to benzene and naphthalene isotherms yielded $n = 1.01 \pm 0.02$ and 0.98 ± 0.02 respectively, confirming the first-order desorption kinetics. Coronene and ovalene, on the other hand, follows fractional-order desorption kinetics, as indicated by a slope of $n = 0.27 \pm 0.04$ and 0.34 ± 0.01 , respectively. The activation energy of desorption and the pre-exponential frequency factors are obtained from intercepts of the isothermal plots. Using Eq. (4.8), the intercept, I , of isothermal plots is solved to be:

$$I = \ln(\nu) - \frac{E_d}{k_B T}. \quad (4.9)$$

Thus, a plot of *intercept* versus $1/T$ can be constructed and a linear fit to this intercept data yields the activation energy and pre-exponential factors from the slope (E_d/k_B) and intercept ($\ln \nu$), respectively. Figure 4.13 displays a representative intercept plot for the isotherms corresponding to benzene desorption. The calculated values of activation energies and pre-exponential factors are shown in Table 4.4. The activation energies and pre-exponential factors calculated by the peak maximum and the isothermal desorption methods are in good agreement with each other within the experimental errors. Major uncertainties in the activation energies obtained using the Redhead method arises from large error bars in the corresponding pre-exponential factors, which comes from the extrapolation of the vapor pressure

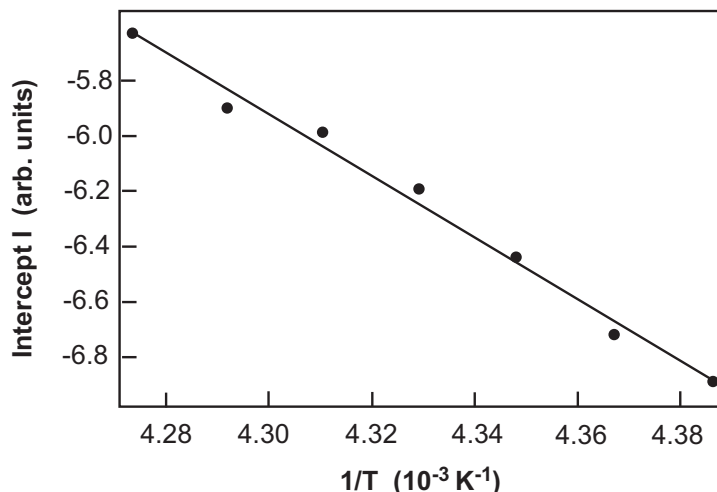


Figure 4.13.: Intercept plot (I versus $1/T$) for benzene desorption from HOPG obtained from the fit to desorption isotherms and respective temperatures (see Fig. 4.12).

data. The small errors in temperature measurement as well as in the coverage calibration also forms a minor contribution. From the binding energies of PAHs, it is evident that all PAH molecules are held on graphite surface by weak van der Waals interaction [Vidali et al., 1991]. The pre-exponential frequency factors calculated from the Falconer-Madix method shows that they are significantly larger than those compared to commonly used values for smaller molecules (10^{12} to 10^{15} s^{-1}). This reinforces the necessity to determine these parameters accurately and reliably, either from experiments or by complementary theoretical investigations, as reported by Fichthorn and Miron [2002]. The high pre-exponentials found here can be qualitatively accounted for by large differences between the partition functions in the adsorbed state and the transition states, in comparison to desorption of mono- or diatomic adsorbates.

4.2.3. Dependence of PAH binding energies on static polarizabilities

In its most generalized form, the van der Waals interaction potential between a neutral molecule and a solid surface has components involving a dispersive (V_d), an induction term (V_i) and an orientation (V_o) terms [Israelachvili, 1992]:

$$V_{vdW} = V_i + V_o + V_d. \quad (4.10)$$

However, when the interaction of neutral molecules without a permanent dipole moment, such polyaromatic hydrocarbons is considered, the dispersive term, V_d , represents the most significant contribution, and the contributions from the induction and orientation terms can be neglected. The origin of this dispersive interaction,

as pointed out in the beginning of this chapter, is understood in terms of attraction from mutually induced dipoles that arises when a neutral molecule approaches a solid surface. In this section, I correlate the activation energy of PAH desorption with dispersive interactions (V_d) which develop when a PAH molecule approaches a graphite surface. From this interaction, the dependence of PAH binding energies on the molecular static polarizabilities can be obtained.

For two neutral species, A and B, the dispersive forces that originate when they approach each other can be expressed in terms of their molecular static polarizabilities, α_A and α_B , respectively [Israelachvili, 1992]:

$$V_d \propto \alpha_A \alpha_B. \quad (4.11)$$

By expressing the experimentally determined activation energy, E_d , of PAHs on graphite surface as a contribution from the adsorbate-substrate interaction (E_{a-s}) and the adsorbate-adsorbate interaction (E_{a-a}), we have [Ulbricht et al., 2004]:

$$E_d = E_{a-s} + E_{a-a}. \quad (4.12)$$

As pointed out in section 4.2.2, the contribution of the adsorbate-adsorbate interaction can be neglected because of the large mutual separation in smaller PAHs, or due to the relatively weak lateral interaction of two-dimensional islands of larger PAHs. That is, if the orientation of PAH molecules is considered to be parallel to the graphite surface, then the interaction potentials on the right-hand-side of the Eq. (4.12) become the only contributions to the dispersive potentials. Thus, the activation energy of desorption of PAHs can be expressed as [Israelachvili, 1992],

$$E_d \propto \alpha_A \alpha_B, \quad (4.13)$$

where α_A and α_B are mutual static polarizabilities of the PAH and the graphene sheet, respectively. Here, it is assumed that the equilibrium distance of the four PAHs from the graphite surface is nearly constant. This implies that if the binding energy contribution arises from only dispersive interactions, the binding energy must be a linear function of the respective molecular static polarizability. Static polarizability of molecules are tensors, and thus, they are anisotropic for all but spherical molecules. In general, they have a form: $\langle \alpha \rangle = 1/3 (\alpha_{xx} + \alpha_{yy} + \alpha_{zz})$, where the first, the second and the third terms correspond to x , y , and z -components of the tensor. For monolayers of large planar molecules such as PAHs, extremely anisotropic polarizabilities remain as an important driving force for favorable mutual orientation [Marčelja, 1973]. Therefore, when considering the dependence of the activation energy of PAH desorption on molecular static polarizabilities, I use the z -component of the polarizability tensor. The polarizabilities of benzene, naphthalene and coronene are obtained from semi-empirical studies presented in the literature [Lu and Lee, 1993]. For ovalene where no theoretical data are available, the static

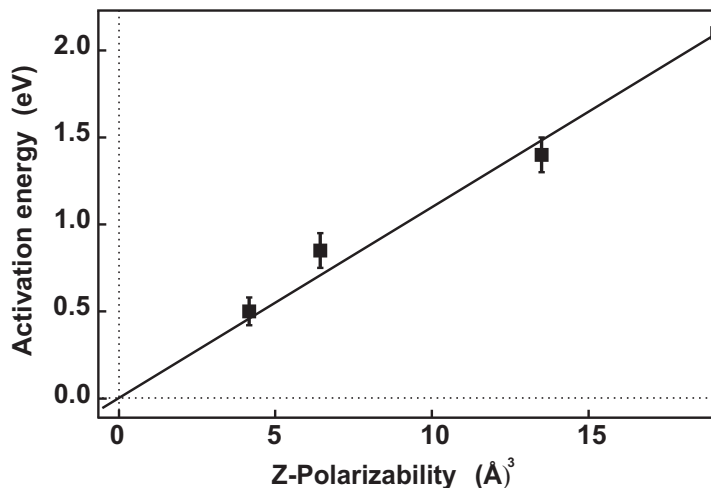


Figure 4.14.: Zero-offset linear dependence of the activation energy of desorption with molecular static polarizability of PAHs.

polarizability is obtained from an empirical bond polarizability model [Guha et al., 1996]. This method is based on expressing the static polarizability as a sum of individual bond polarizabilities. Polarizabilities of PAH molecules calculated from known values of individual carbon-carbon and carbon-hydrogen bonds (i.e., C—C, C=C and C—H bonds) in general give excellent agreement with the experimentally obtained polarizabilities and, thus, are used to calculate the static molecular polarizability of ovalene. The molecular static polarizabilities for all four PAH molecules are displayed in Table 4.2.

From Fig. 4.14, the PAH binding energies are found to be linearly dependent on molecular polarizability. Also the binding energy vanishes when extrapolated to zero polarizability, which is in confirmation within the united-atom model of adsorbate-substrate interactions [Ryckaert and Bellemans, 1978]. A number of studies that measured the desorption kinetics of linear and cyclic hydrocarbon molecules indicated a linear dependence of binding energy with number of carbon atoms, however with a non-zero intercept [Lei et al., 2004; Paserba and Gellman, 2001a,b]. Similarly, a non-zero offset linear dependence of binding energy on the molecular static polarizability of long-chain hydrocarbon molecules has been reported by Lei et al. [2004]. This anomalous scaling of binding energy was attributed to factors such as lattice commensurability effects, temperature and desorption order. However, in these studies, the determination of the activation energy of desorption was made using a fixed pre-exponential frequency factor. Also, when the polarizability of the long chain hydrocarbon molecules are dealt in those studies, they failed to account for the anisotropic nature of the polarizability and therefore overestimated its contribution to the binding energy. Our present study indicates that the binding energies of hydrocarbon molecules scales linearly with number of carbon atoms and also with

the z -component of the molecular static polarizability which is in agreement with the predictions within the united-atom model [Fichthorn and Miron, 2002]. From the linear dependence and the apparently vanishing offset when extrapolating to zero polarizability, one can deduce that the PAH molecules are held on the graphite surface by only dispersive interactions, and the contributions of other terms are negligible. Due to the similarity between a larger PAH and the graphene sheet, therefore, it can be argued that the dispersion observed in the graphite arises solely from the van der Waals interaction between the layers.

4.3. Interlayer cohesive energy of graphite

The cohesive energy of a solid is known as the energy required to disassemble it into its constituent atoms, while the energy required to separate unit areas of a medium from contact to infinity is referred to as the work of cohesion [Ashcroft and Mermin, 1976; Israelachvili, 1992]. These two energies are not identical, and for a layered system with extremely anisotropic bonding like graphite, the first can be identified as the exfoliation energy E_{ex} , i.e., the energy required to separate all layers of graphite to infinity, while the latter is equivalent to cleavage energy E_{cl} , which is slightly larger than the exfoliation energy [Girifalco and Lad, 1956]. To calculate the interlayer cohesive energy, here normalization of binding energies are performed with respect to surface atoms (i.e., the constituent parts) and not to unit area, which then corresponds to cohesive energy. For a graphene sheet, the area per surface atom is $1.05 \times 10^{-19} \text{ m}^2$ [i.e., $\sqrt{3} \times (2.46 \times 10^{-10} \text{ m})^2$].

4.3.1. Determination of carbon-carbon interaction potential

The underlying assumption on which the calculation of interlayer cohesive energy is made is the near-additivity of long-range van der Waals interaction [Margenau, 1939]. This additivity of vdW interactions is clearly demonstrated, in the calculation of cohesive energies of long chain alkanes, where the deviation from the linearity is 1 % or less [Israelachvili, 1992; Lii and Allinger, 1989]. In order to calculate the interlayer cohesive energy, the activation energy of desorption — as obtained from analysis of thermal desorption spectra — is identified here with the binding energy of the respective adsorbate to the graphite surface (This is true for the energetics of physisorption, see chapter 2). Based on the above additivity principle, the contribution of individual carbon atoms to this binding energy — in the limit of infinitely large PAHs — would correspond to the energy needed to separate a graphene sheet from its parent crystal. Additional contributions from intermolecular interactions are negligible, either due to large adsorbate-adsorbate separation in the case of smaller PAHs or because of weak adsorbate-adsorbate interaction within two-dimensional islands in comparison to adsorbate-substrate interaction in larger

PAHs and thus, they are ignored [Vorpapel and Lavin, 1992].

A rough estimate of the exfoliation energy can be obtained by averaging over binding energies per carbon atom for all studied adsorbates, which would yield a value of 67 meV/atom. In this case, however, one neglects the small but significant contribution to the binding energy from hydrogen atoms. Hence, this naive approach overestimates the contribution of carbon atoms to the total binding energy. A more thorough analysis has thus to account for the contribution of hydrogen atoms. Here, this is done by optimizing carbon-carbon and carbon-hydrogen interaction potentials so as to obtain the best agreement of experimental binding energies with calculated values. Experimental data for this optimization are obtained by averaging values obtained from the Redhead and the Falconer-Madix methods.

The calculated binding energies are obtained by summing over empirical vdW pair potentials:

$$E_B^{\text{PAH}} = \sum_{n,m} V^{\text{CC}}(|r_n - r_m|) + \sum_{l,m} V^{\text{HC}}(|r_l - r_m|), \quad (4.14)$$

where the summation over n and l includes all carbon and hydrogen atoms in the adsorbate and the summation over m includes all atoms in the substrate. In the above equation, the carbon-carbon and carbon-hydrogen vdW potentials are those given by MM3 force field potentials from Lii and Allinger [1989]. They have the form:

$$V^{\text{AB}}(r) = \epsilon_{\text{AB}} \left[184000 \exp \left(-\frac{12r}{r_{\text{AB}}} \right) - 2.25 \left(\frac{r_{\text{AB}}}{r} \right)^6 \right]. \quad (4.15)$$

Here, ϵ is an energy scaling factor for each atom pair which measures the interaction energy. r_{AB} is the van der Waals distance and r is the effective distance between interacting centers of two atoms. For dissimilar A and B atoms, ϵ_{AB} is given by $\epsilon_{\text{AB}} = \sqrt{\epsilon_{\text{A}}\epsilon_{\text{B}}}$ and r_{AB} is given by $r_{\text{AB}} = r_{\text{A}} + r_{\text{B}}$. Here I use the values $(\epsilon_{\text{C}}, r_{\text{C}})$ and $(\epsilon_{\text{H}}, r_{\text{H}})$ for carbon and hydrogen as given by Lii and Allinger [1989]: (2.44 meV, 1.96 Å) and (0.87 meV, 1.67 Å), respectively.

Calculation of the binding energies $E_B^{\text{PAH}}(V_0^{\text{CC}}, V_0^{\text{HC}}, z)$ is done by using the depth of two vdW potentials V_0^{CC} and V_0^{HC} , as free scalable parameters having a fixed position of the potential minima. The best agreement with the experimental binding energy is then obtained by adjusting the molecule-surface distance, z , while the aromatic ring orientation is fixed parallel to the graphite surface. The optimization is then done for the parameters V_0^{CC} and V_0^{HC} for all PAHs, by minimizing the corresponding root mean square deviation. Using the MM3 force field parameters, the depth of the hydrogen vdW potential, V_0^{HC} , for interaction with a graphite surface is estimated to be 27 meV/atom. If this is allowed to vary by at most ± 5 meV, the depth of the carbon-graphite potential is calculated to be 52 ± 5 meV/atom within the best agreement with the experimental binding energy. The plot of the calculated and the experimental binding energies of PAHs are shown in Fig. 4.15. From Fig. 4.15,

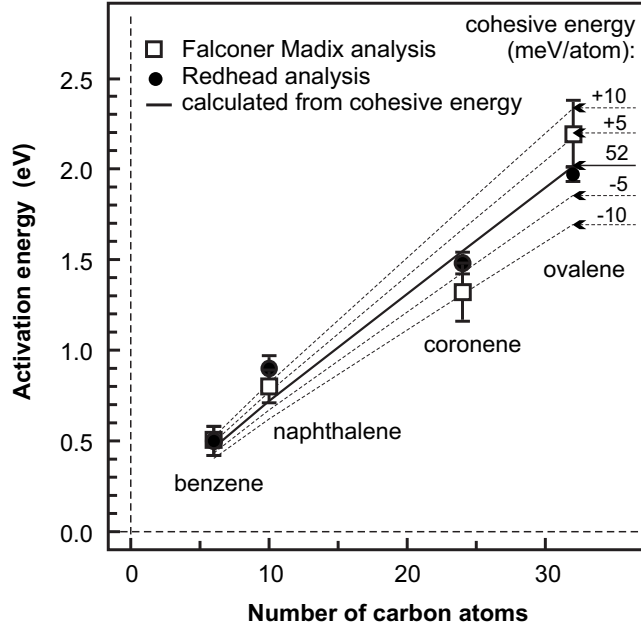


Figure 4.15.: Dependence of activation energy for desorption on the number of carbon atoms from four polyaromatic hydrocarbons. The broken lines show the binding energies per C atom when the hydrogen-graphite vdW potential is varied up to ± 5 meV, while the solid line indicates the best agreement with experimental PAH binding energies.

where calculated and experimental binding energies are compared, one finds that the theoretical and the calculated values are within reasonable agreement, with a deviation of about 10 % or less. The major uncertainty in the experimental values arises from the large error bars in the pre-exponential frequency factors obtained from the Redhead method and the estimated error in the temperature calibration, and the reproducibility of TD traces due to small variations in the measured temperature for the Falconer-Madix analysis. For coronene and ovalene, an additional error typically of about 2 % arises due to uncertainties in the coverage calibration. The cleavage energy, E_{cl} , of graphite is obtained from the above value by accounting for the 18 % higher energy, if compared with the separation of a single layer of graphite from its parent crystal [Girifalco and Lad, 1956]. This yields a cleavage energy of (61 ± 5) meV/atom. As pointed out in the section 4.1.2, the earliest experimental characterization of interlayer cohesive energy was a heat of wetting experiment, which resulted in 43 ± 5 meV per surface atom [Girifalco and Lad, 1956]. However, a systematic comparison of sample-dependent and other uncertainties of this value with our result is difficult, as the nature of the carbon samples used in their experiment is largely unknown [Girifalco and Lad, 1956]. A smaller value of (35^{+15}_{-10}) meV/atom is obtained by Benedict et al. [1998], where the uncertainties are due to limited accuracy in determining the diameter MWNTs which makes it

difficult to make a meaningful comparison to our experimental value. The distinct advantages in our experimental determination is that, a well characterized model system is used for the investigation of graphitic interlayer cohesive energy and the experimental conditions and assumptions leading to our conclusions are most clearly defined.

The strength of the carbon-carbon pair-potential determined in this study is only about 5 % lower than that empirically obtained values in soft matter calculations.

4.4. Summary and outlook

In this chapter, I present an experimental characterization of weak van der Waals interaction in graphite using the thermal desorption spectroscopy of four benzenoid polyaromatic hydrocarbons. Due to the structural and electronic similarities of polyaromatic hydrocarbons with graphitic basal planes, the dispersion of PAHs on graphite is considered to be an apt model system for studying the interaction between basal planes in graphite. The pre-exponential frequency factors and activation energies for the desorption of benzene, naphthalene, coronene and ovalene from graphite surface are obtained from TD spectra using two different methods for analysis: the Redhead's peak maximum and the Falconer-Madix methods. The calculated pre-exponential factors are found to increase with adsorbate size from 10^{15} s^{-1} for benzene to 10^{21} s^{-1} for ovalene. The pre-exponential frequency factors for PAH desorption are found to be significantly larger than those of smaller molecules. This can be qualitatively explained by the suppression of various vibrational degrees of freedom in the adsorbed giant PAH molecules. The binding energy of PAH molecules increase linearly from 0.05 eV for benzene to 2.1 eV for ovalene. The binding energies are found to be linearly scale with the z -component of the molecular static polarizability, and are also found to vanish when extrapolated to zero polarizability. This observation is in agreement with the united-atom model of adsorbate-substrate interactions, and also confirms that van der Waals dispersive interaction is the dominant interaction between PAH molecules and the graphene sheet.

The contribution of a single carbon atom to the PAH binding energy is obtained from the total PAH binding energy by comparing the binding energy of four PAHs which are calculated using MM3 pair potentials for carbon-carbon and carbon-hydrogen interactions. This determination is based on the additivity principle of vdW interactions, i.e., the contribution of individual carbon atoms to a PAH binding energy — in the limit of infinitely large PAHs — corresponds to the energy required to separate a graphene sheet from its parent crystal. The resulting cleavage energy of $(61 \pm 5) \text{ meV/atom}$ is derived from the average binding energy of a PAH, i.e., $(52 \pm 5) \text{ meV/atom}$. The exfoliation energy value obtained in this study is significantly larger ($\sim 42 \%$) than the previously reported experimental value.

